Journal of the Geological Society, London, Vol. **170**, 2013, pp. 833–847. http://dx.doi.org/10.1144/jgs2012-150
Published *Online First* on July 24, 2013

Weathering rinds as mirror images of palaeosols: examples from the Western Alps with correlation to Antarctica and Mars

W. C. MAHANEY[1,2*], LESLIE KEISER[3], D. H. KRINSLEY[4], P. PENTLAVALLI[5], C. C. R. ALLEN[5], P. SOMELAR[6], STEPHANE SCHWARTZ[7], JAMES M. DOHM[8], R. DIRSZOWSKY[9], ALLEN WEST[10], P. JULIG[11] & P. COSTA[12,13]

[1]*Present address: Quaternary Surveys, 26 Thornhill Ave., Thornhill, ON L4J 1J4, Canada*
[2]*Department of Geography, York University, N. York, ON M3J 1P3, Canada*
[3]*Department of Geological Sciences, University of Oklahoma, Norman, OK 73019-1009, USA*
[4]*Department of Geological Sciences, University of Oregon, Eugene, OR 97403-1272, USA*
[5]*Queen's University Belfast, School of Biological Sciences, Belfast BT7 1NN, UK*
[6]*Institute of Ecology and Earth Sciences, University of Tartu, Tartu, Estonia*
[7]*Université Grenoble 1 ISTerre-UMR 5275, F-38041, Grenoble, France*
[8]*Earth–Life Science Institute, Tokyo Institute of Technology, Meguro, Tokyo 152-8551, Japan*
[9]*Department of Earth Sciences, Laurentian University, Sudbury, ON, P3E 2C6 Canada*
[10]*GeoScience Consulting, Dewey, AZ 86327, USA*
[11]*Department of Anthropology, Laurentian University, Sudbury, ON, P3E 2C6 Canada*
[12]*University of Lisbon, Department of Geology, Lisbon, Portugal*
[13]*Department of Geography, University of Dundee, Dundee DD1 4HN, UK*
**Corresponding author (e-mail: arkose@rogers.com)*

Abstract: Weathering rinds have been used for decades as relative age indicators to differentiate glacial deposits in long Quaternary sequences, but only recently has it been shown that rinds contain long and extensive palaeoenvironmental records that often extend far beyond mere repositories of chemical weathering on both Earth and Mars. When compared with associated palaeosols in deposits of the same age, rinds often carry a zonal weathering record that can be correlated with palaeosol horizon characteristics, with respect to both abiotic and biotic parameters. As demonstrated with examples from the French and Italian Alps, rinds in coarse clastic sediment contain weathering zones that correlate closely with horizon development in associated palaeosols of presumed Late Glacial age. In addition to weathering histories in both rinds and palaeosols, considerable evidence exists to indicate that the black mat impact (12.8 ka) reached the European Alps, a connection with the Younger Dryas readvance supported by both mineral and chemical composition. Preliminary metagenomic microbial analysis using density gradient gel electrophoresis suggests that the eubacterial microbial population found in at least one Ah palaeosol horizon associated with a rind impact site is different from that in other Late Glacial and Younger Dryas surface palaeosol horizons.

Weathering rinds have a long history of use in clast relative-age assessment especially in Arctic, Antarctic, and alpine terrain (Sharp 1969; Birkeland 1973; Chinn 1981; Mahaney 1990; Ricker *et al.* 1993; Laustela *et al.* 2003). Apart from recent work in direct rind dating using U-series nuclides (Pelt *et al.* 2003), which greatly refines the method of using rind thickness alone as a chronometric tool, little attention has been paid to the wealth of palaeoenvironmental information recorded in terrestrial rinds developed in various lithological species. Some researchers have focused recently on moisture as a mechanism of microweathering (Thorn 1975), as a control of oxidation and hydrolysis leading to rind growth between rock walls and near planar bedrock (Nicholson 2008, 2009), and as a significant factor in developing diffusion models to explain rates of basalt or andesite weathering (Oguchi & Matsukura, 2000; Oguchi 2004; Sak *et al.* 2004; Navarre-Stichler *et al*. 2011). Mahaney *et al.* (2012*a*,*b*, 2013*a*) studied rind growth using high-resolution scanning electron microscopy (SEM) to image not only country rock but also allochthonous materials, including organic compounds, with chemistries determined by energy-dispersive spectrometry (EDS), and thereby discovered that detailed palaeoenvironmental archives lay buried in rind successions on Mount Kenya. Rind studies focusing on transects of chemical weathering reveal a parallel microcosm similar to 'wetting depths' in palaeosols, with micro-horizon genesis in rinds closely correlated with horizon genesis in palaeosols. Weathered zone genesis within rinds in cold climates and associated fossilization of biotic materials are underappreciated aspects of rind growth as coarse clastic fresh material is transformed into weathered regolith (palaeosols).

Rock coatings in arid and cold climates have been researched (Dixon *et al.* 2002; Dorn 2009; Langworthy *et al.* 2011), mainly to assess geochemical processes of dissolution and precipitation at the nanometre level. However, following deposition of coarse clastic materials and exposure over varying lengths of time, rinds may extend many millimetres into rock, eventually converting much of the rock fabric into clay grade material and a variety of alteration products (Mahaney *et al.* 2012*a*,*b*, 2013*a*; Mahaney & Keiser 2013). In one of the few attempts to determine clay mineral content in rinds, Dixon *et al.* (2002) failed to identify any clay species in rock rinds of northern Scandinavia, whereas tropical alpine rinds of

extreme age (*c*. 2.0 Ma) are known to contain metahalloysite (Mahaney *et al.* 2012*a*). The Mt. Kenya study showed the range of bioweathered products in rinds of Late to Early Pleistocene age in the tropical Afroalpine environment, a starting point that led to the application of these findings to older, well-weathered coarse clastic sediment in Antarctica with applications to Martian terrain (Mahaney *et al.* 2012*b*). Others, particularly Etienne (2002), have argued for rapid microbe development in rinds (*c*. 100 years) in Icelandic basalt clasts without considering the possibility of clast reworking from previous weathering episodes of longer duration. Previous studies (Mahaney *et al.* 2012*a*, 2013*a*) of microbe genesis and fossilization in phonolites on Mt. Kenya, a tropical Afroalpine environment, have shown that identifiable bacteria and fungi first appear in clasts older than the Last Glacial Maximum (LGM).

Meteorites encountered by the Mars Exploration Rover (MER) Opportunity on Meridiani Planum (Fairén *et al.* 2011) exhibit evidence of long-lived weathering (*c*. 1 Gyr), presumably in an aqueous palaeoenvironment during the Noachian Period (*c*. 4 Ga). Deep cavernous weathering of six meteorites encountered on Mars is similar to observations of weathered clasts in the Antarctic (Mahaney *et al.* 2012*b*), and provides the first close-up study of Fe-rich clasts under a palaeo-atmosphere considered similar to that of early Earth. Because these clasts are considered to have been buried after a *c*. 1 Gyr weathering event, prior to later exhumation and eventual encounter with the Opportunity rover, they were probably later subjected to minor chemical alteration in the cold, dry Martian Amazonian climate for an inestimable amount of time (Ashley *et al.* 2011). Despite the imprecise details of emplacement, weathering, burial, exhumation and subsequent weathering in an Antarctic-like environment, the Meridiani Planum meteorites were exposed first to warmer climate, followed by burial for an unknown, but long period of time, with subsequent exposure later to a colder surface climate that progressively worsened, the sum of which produced etched microfeatures akin to microfeatures observed on Antarctic clasts of Middle Miocene age. Given the wealth of mineral weathering products and biota archived in terrestrial rinds, as described above and discussed herein, there is clearly considerable latitude for future rind investigations on the Red Planet and on Earth. Even nanoscale studies on asteroids such as Itokawa reveal the presence of water in the past and plentiful Fe-rich minerals that may have fostered growth of fossil microbes (Mahaney *et al.* 2009). Given that rind weathering zones and palaeosol horizons on Earth can be correlated, there is a distinct possibility that similar correlations may be possible on Mars once exploration of the planet begins on a scale suitable to recover palaeosol profiles.

Antarctic rinds, as proxy indicators of clast weathering on Mars, are known only from the work of Mahaney *et al.* (2012*b*), with analysis limited to the depth of solution pits in granite, sandstone and dolerite. Although the time frames between slow weathering in the Antarctic (i.e. *c*. 20 Myr), weighed against faster weathering (*c*. 15 kyr) in the middle-latitude alpine environment of the Alps, make it difficult to assess rind development as age indicators between the two environments, it is evident that there is clear palaeoenvironmental archival information contained in both databases. By extension, it is possible to infer that similar palaeoenvironmental archives may be present in Martian clasts (Fairén *et al.* 2011), and these may also correlate with resident palaeosols, which would extend the rind weathering record into the Noachian (*c*. 4 Ga), far earlier than on Earth.

The intricate and complex nature of weathering zones in terrestrial rinds compared with large-scale horizon development in palaeosols of the Western Alps of France and Italy is the subject primarily discussed herein. Because the black mat event of 12.8 ka (Mahaney & Keiser 2013) is considered a Younger Dryas boundary (YDB) marker for the inception of the Younger Dryas (YD) cosmic impact event, and because evidence for such an impact is resident in both surface clast rinds and palaeosols, attention is directed here to the impact event in the Western Alps and its role in both rind and palaeosol evolution. The broader aspect of this investigation is the degree to which other workers may find weathering rinds to contain a microcosm of palaeoenvironmental history written into the nanoscale record of surface clasts embedded in deposits with various provenances. Weathering records, in some cases, may correlate closely to the macroscale record in associated palaeosols and may not be confined to the terrestrial sphere, as forthcoming missions to Mars may profit from exploration of exposed surface clast or rock outcrops that may contain records of extreme longevity, perhaps dating to the origin of the planet (Mahaney *et al.* 2012*b*). Moreover, in addition to chronometric indicators discussed by Gordon & Dorn (2005), weathering rinds offer archival information important in climate change, global warming, rock art preservation, and building conservation research.

Regional geology

The Guil River catchment (Fig. 1) is a linear fault-controlled glacial basin with headwaters on the western slopes of Mt. Viso (3841 m above sea level (a.s.l.)) adjacent to the France–Italy border. The upper Guil catchment is considered the type locality of a cosmic impact in the European Alps, evidence for which was first uncovered during analysis of local weathering rinds in 2008 (Mahaney & Keiser 2013). Throughout the narrow and wide sections of the catchment, the valley is floored with bedrock and recent alluvium with talus, solifluction terraces and successive debris flows. Whereas active glacial erosion is evident on both the north- and south-facing valley slopes, recessional moraines are non-existent, which clearly indicates that retreat of Late Glacial (Würm–Weichselian) Guil ice from the Durance valley (where it fed into the larger Durance Glacier) was rapid. Hence, stillstands of Late Glacial (LG) ice were probably short lived. Some carbon, resident in the impact-affected clasts embedded in Late Glacial deposits, may have been sourced from sparse vegetation and associated thin Entisols (National Soil Survey Center 1995; Birkeland 1999) of the alpine grassland when an high-temperature cloud descended upon the area producing a conflagration that would have destroyed all life, including plants in what was probably a wet tundra in its early developing seral stage (Mahaney & Keiser 2013).

Prominent recessional moraines are found only at one location within the Guil drainage, located *c*. 1 km from the drainage divide (2400–2450 m a.s.l.). The innermost recessional moraines were overrun by a glacial readvance, presumed to be the YD. Because palaeosol development and weathering properties of coarse clastic debris on these LG and YD deposits are similar, they must have an age separated by centuries or possibly a millennium. Above the LG and YD moraine limits steep slopes lead into a prominent cirque (below the Col de la Traversette *c*. 3000 m a.s.l.; Mahaney 2008), largely characterized by Little Ice Age rockfall and talus cover and devoid of ground moraine. Although it is impossible to determine if LG ice receded into the Traversette cirque prior to the YD, it is unequivocally the case that the YD ice advanced to 2450 m at a later date, overrunning the inner LG recessional moraine.

At the end of the last glaciation, ice first retreated up the Guil valley toward Mt. Viso, the main ice sheet dividing into separate glaciers retreating into the Traversette cirque and an unnamed cirque to the south below the summit of Mt. Viso (Fig. 1). Following the YDB the situation reversed, with the advent of the YD cooling

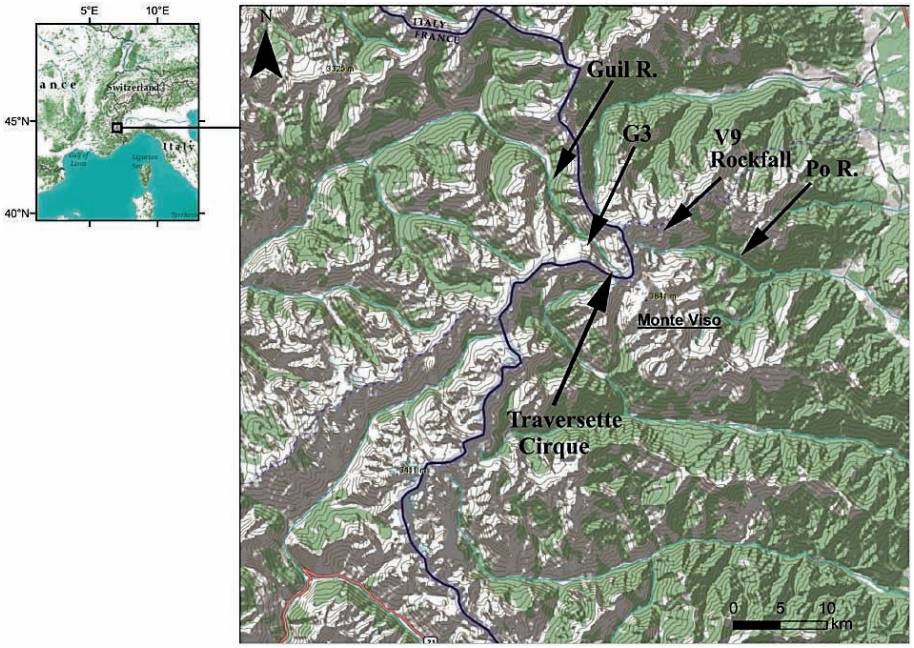

Fig. 1. Location of GUIL3 (G3, upper Guil catchment) and VISO9 (V9, upper Po River catchment) sites, Mt. Viso area, Western Alps, France and Italy.

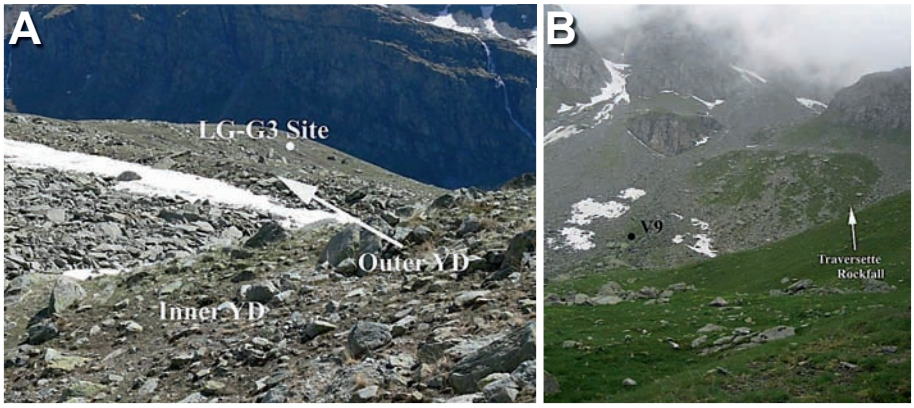

Fig. 2. (**a**) Field area in the Upper Guil River showing positions of G1 and G2 (YD moraines) and G3 (Late Glacial recessional moraine). (**b**) Location of V9, oldest lobe in the Traversette rockfall.

event and onset of positive glacial mass balance in the upper valleys causing renewed glaciation, which left a wealth of glacial geomorphological and sedimentological evidence. The LG stillstand recessional moraines provide coarse clastic debris as host material for weathering rind development, part of which contains evidence of a cosmic impact, presumably the progenitor of the YD climatic reversal. As the latest event in the Late Glacial record (Ralska-Jasiewiczowa *et al.* 2001; Gibbard 2004), the YD occurs on the upper end of a warming trend initiated at 14.7 ka (Vanderhammen & Hooghiemstra 1995; Teller *et al.* 2002; Lowe *et al.* 2008), with the maximum cooling initiated at 12.8 ka. The hypothesis that the cosmic impact could have generated the YD reversal is still vigorously debated in the literature (Kennett *et al.* 2007, 2009; Pinter & Ishman 2008; Vance Haynes 2008; Ge *et al.* 2009). Recent critical reviews of the YD event by Vanderhammen & Van Geel (2008) and Broecker *et al.* (2010) argued, respectively, that charcoal in palaeosols of the Allerød–YD transition were not caused by impact and that the black mat event, by itself, could not have caused a glacial advance lasting 1 kyr.

All glacial or fluvial outlets in the research area drain across steep gradients (10–35° slopes) into the Guil River and these do not contain terraces of LG age that might carry a record of the cosmic impact. Cores (unpublished) retrieved from a mire within the YD moraine belt reveal only a Middle Holocene record beginning *c*. 4 ka.

The criteria for the YD impact are similar to evidence used to prove the K–T impact (Hildebrand 1993), with the exception that the alpine locality is in metamorphic terrane, which was under glacier recession at the time of impact. The deposits investigated are located at 2450 m a.s.l. in the upper Guil catchment and 2300 m a.s.l. in the upper Po catchment (Fig. 1), both sites being in Late Glacial-age sediment. The impact evidence is in pebble size clasts on the inner LG recessional moraine (G3) located in front of a doublet moraine of presumed YD age (Fig. 2a) and in surface clasts at the V9 site (Fig. 2b). Although ^{14}C dates are not available for the LG (G3 site) and YD moraines, the outer YD moraine buries part of the inner LG recessional moraine (Fig. 2a), clearly the result of a glacial readvance. The lack of lakes or bogs suitable for coring makes it almost impossible to find sites with resident impact beds still intact, clasts on LG moraine and rockfall deposits and palaeosols being the only repositories of the cosmic impact discovered to date in the French and Italian Alps.

Materials and methods

Deposits were mapped from 1:20000 air photographs and sites were selected on the basis of representative soil expression. Clasts embedded in major landforms, including those shown in Figure 2a and b, were sampled for rind counts and lichen measurements, with corresponding soil pits being established in each case. Rinds tend to be thicker on the upper surface exposed to the atmosphere, and somewhat thinner on surfaces embedded in Ah soil horizons. Previous work by Thorn (1975) indicated that rind thickness may reflect position in deposit surfaces.

Pebbles of uniform lithology were collected from moraine surfaces and cracked with a rock hammer, and weathering rinds were measured to the nearest millimetre perpendicular to the pebble surface inward to the fresh lithic core. The rinds indicate the degree to which Fe-bearing minerals oxidize and discolour the outer periphery of clasts, and their thickness is used as an estimate of time since deposition (Birkeland 1973; Mahaney 1990). Whereas many workers measure only the maximum thickness of discoloration (oxidation of Fe-bearing minerals), neglecting the irregular thickness found in most clasts, we measured both maximum and minimum rind dimensions on each clast (Mahaney 1990). The maximum rind is defined as the maximum discoloration measured in the outer surfaces of a population of 50 pebbles of similar lithology at each site. The minimum rind is the minimum thickness for the same 50 specimens. The populations of maximum and minimum rind thicknesses are then subjected to a means test, the mean maximum value being used to approximate maximum weathering at a site and the mean minimum value indicating the lesser penetration of reacting fluids. Usually the maximum rind is in the clast surface in contact with the subaerial atmosphere and/or lichen cover, and the minimum occurs in contact with the underlying soil or palaeosol.

Selected rind subsamples were mounted on stubs for analysis by SEM (SE), BSE and EDS following the methods outlined by Mahaney (2002). Because carbon is important in this analysis, samples were coated with gold–palladium (Vortisch *et al.* 1987; Mahaney, 2002). Photomicrographs were obtained at accelerating voltages of 20 keV. X-ray microanalysis was acquired at an accelerating voltage of 20 keV.

Soil and palaeosol descriptions follow standard protocol established by the National Soil Survey Center (1995). The 'Cox' horizon designation as defined by Birkeland (1999) highlights C horizons with detectable levels of secondary Fe hydroxides and oxides, whereas 'Cu' refers to unweathered parent material (Hodgson 1976). The 'Ah' designation is applied where sufficient colour strength indicates appreciable humus (Canada Soil Survey Committee 1977). Soil colours were assigned using the soil colour chips of Oyama & Takehara (1970). Approximately 300 g samples were collected from single soil horizons for particle size, clay mineral, geochemical and microbiological analyses. Samples were air dried and treated with H_2O_2 to oxidize organic material. The samples were then wet sieved, and the <63 μm fraction was subjected to analysis by hydrometer (Day 1965). Particle grade sizes are based on the Wentworth Scale with the exception of the clay–silt boundary (2 μm), which follows the US Department of Agriculture definition. Organic carbon was determined by loss on ignition, and total salts by electrical conductivity. The geochemistry was determined by neutron activation at Activation Laboratories Ltd, Ancaster, Ontario.

The clay fraction was studied for mineral composition by means of powder XRD using a Bruker 8D diffractometer with Ni-filtered CuKα radiation. Scanning steps for oriented samples were 0.02° 2θ from 2 to 55° 2θ. A semi-quantitative mineral composition was determined from peak integral intensities of chlorite, illite–vermiculite, mica + illite, kaolinite, talc and smectite, multiplied by factors of 1, 0.35, 2, 1.4, 0.2 and 0.2, respectively (Kalm *et al.* 1997).

Finally, separately collected samples of Ah, Bw, C/Cox and Cu horizons of the G3, V9 and additional moraine deposits were subjected to preliminary metagenomic microbial analysis. Sediment samples were taken under aseptic conditions for this purpose from the mid-point depth of respective soil horizons. Cu horizons were sampled *c*. 5 cm below the top of the horizon. The samples were frozen and stored at −20 °C upon return to the laboratory. Sediments were subject to total DNA extraction (Griffiths *et al.* 2000) and subsequently compared using density gradient gel electrophoresis (DGGE) analysis of 16S rRNA gene partial sequences (Muyzer *et al.* 1993). The 16S rRNA gene is present in all bacterial isolated DNA, and as a 'housekeeping gene' has been widely used to define microbial phylogeny. Here populations of this gene in different samples were compared to assess the similarity between bacterial communities found between sites and within soil profiles. Statistical analysis of DGGE results was performed using cluster analysis based upon the unweighted pairwise grouping method with mathematical averages (UPGMA).

Results

Weathering rinds

Weathering rinds in a metabasalt clast at site G3 on the Late Glacial moraine surface shown in Figure 1 exhibit maximum thicknesses ranging from 1 to 5 mm, yielding a mean maximum value of 2.90 mm, based on a population of 50. Approximately 15% of all clasts collected for measurement were nearly shot through with weathering, as preweathered samples, and were discarded in the analysis. The minimum rind thicknesses ranged from 0 to 2 mm, and the mean minimum rind value (n = 50) reached 0.56 mm, with 44% of the total population registering positive values and 56% values of zero. These results are similar to those for mean maximum and mean minimum rinds measured on nearby YD moraines (G1 and G2, Fig. 2a), the difference in age and weathering time since time zero not being sufficient for us to expect measurable variation.

Rinds at V9 on the oldest exposed and uneroded rockfall lobes of the Traversette Rockfall (Fig. 2b) show maximum thicknesses ranging from 1 to 5 mm, with mean maximum rind values of 3.04 mm, similar to those for G3 above and also based on a population of 50 clasts. Minimum rind thicknesses at the V9 site range from 0 to 1 mm, with a mean minimum thickness of 0.18 mm, considerably smaller than the values for G3. Of the 50 V9 clasts measured, only 18% yield minimum thicknesses greater than zero. Macrophotography of selected rinds is shown in Figure 3; their maximum and minimum thicknesses are close to the mean values calculated from the field data. As illustrated in Figure 3, the rinds exhibit weathering zones that correlate with Ah, Bw and C, and sometimes Cox horizons in palaeosols at the G3 and V9 sites (Fig. 4). Although direct chemical comparisons are lacking, colour variations strongly indicate that weathered zones in the rind database contain organic residue on the clast surface, which is from past lichen or plant growth material that is probably slowly being oxidized. Beneath the micro-thin 'Ah' zones, a 'Bw' weathered area is a close micro-correlative to the Bw palaeosol horizon and probably contains a concentration of secondary oxides and hydroxides similar to what is in the palaeosol. Lastly, and with greater depth in the rind, a C or Cox correlative horizon exists as a transition zone extending to a sharp contact with the fresh lithic interior. Although these zones are discontinuous they are common in most of the clasts sampled at both sites.

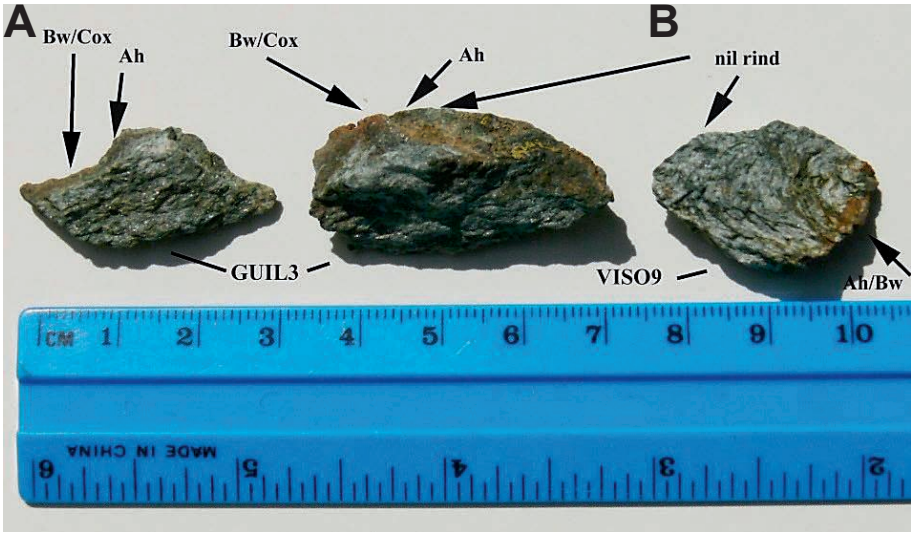

Fig. 3. Macrophotographs of GUIL3 (hereafter G3) and VISO9 (hereafter V9) rinds. (**a**) G3 rind showing correlative palaeosol horizons Ah/Bw/Cox. (**b**) V9 rind showing similar correlative palaeosol horizons.

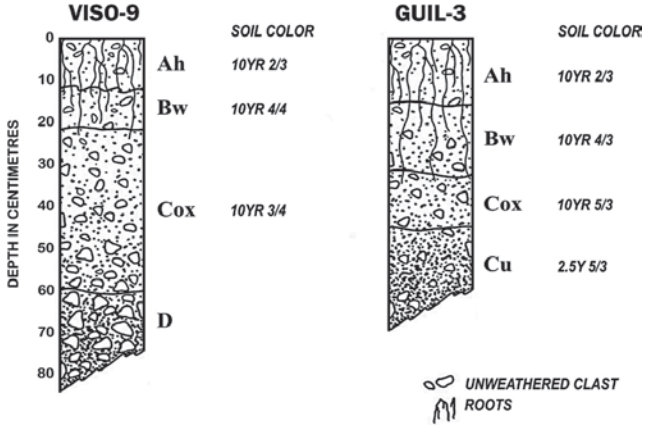

Fig. 4. Palaeosol profiles G3 and V9, all of Late Glacial, pre-Younger Dryas age.

Rind microscopy

Preliminary examination under the optical microscope of rinds recovered from G3 and V9 reveals highly brecciated outer rinds, twisted, contorted and melted quartz and feldspar grains, and relatively thick, opaque carbon sheets and spherules welded to grains within the rind. A low-magnification SEM image shows the characteristic rind character (Fig. 5a) from the outer zone area toward the interior, with a more complex mineralogy dominated by melted quartz, zircon, olivine, pyroxene and Ca-plagioclase. Also, the bubbled (vesicular) character of the carbon, which is characteristic of high temperatures, should be noted. Tonal contrasts in the SEM image indicate the approximate distribution of C and Fe, with lighter tones characteristic of Fe and darker tones characteristic of carbon. Although clearly minor in concentration, zircon, an impact melt-product, is possibly allochthonous, although it could be an aeolian short- or long-distance delivery product. A higher resolution image (Fig. 5b) of the outer breccia zone in the Guil3 rind reveals small and very angular shards of debris, partially melted in places, and heavily coated with thick carbon coatings indicated by the darker colour, with microfeatures similar to those shown in Figure 5a. The brecciation and melting of mineral grains combined with the carbon features observed are similar to those of grains previously described and analysed by Mahaney *et al.* (2008, 2010, 2011*a*, 2011*b*) and representative of the black mat in the Venezuelan Andes. It is possible that some carbon coatings contain the characteristic glassy carbon spherules common in the black mat in North and South America (Bunch *et al.* 2012) but finding such material would require more refined analysis than was possible in this instance.

Additional high-resolution imagery and chemical mapping (Fig. 6) shows the extensive spatial distribution of unmelted and melted grains within the rinds. A majority of these are quartz, requiring melting temperatures up to >1600 °C. In this image, quartz, pyroxene and Ca-plagioclase dominate as principal mineral species, and their distributions are confirmed largely by chemical mapping. Carbon is widely distributed across the sample, mostly in a diagonal pattern from centre to right. Where its thickness exceeds 1 μm, identification of minerals deeper in the sample is largely precluded by the carbon thickness. Melted, folded diaphanous sheets of material, present along the light-coloured diagonal, are an undifferentiated mix of mainly C, Si and Fe. Sequestered Si, Fe, Mg and Ca in the lower left of this sample are probably related mainly to the presence of pyroxene (and lack of carbon). The Cl concentration, although not accompanied by Al, could correlate to Cl-enriched Al glass or to Cl ablation out of a descending cosmic cloud. High Ti in the low border area of the sample may indicate the presence of rutile or anatase or both, although the Ca content suggests that the mineral may be titanite. Rutile, often a partition mineral (Ryerson & Watson 1987) in alkaline basalts, may, in this case, be part of the country rock.

Imagery of the outer and middle section of the V9 rinds (Fig. 7a) shows cracks in the mineral fabric, which again are filled with melted grains that may have attained fluidity as a result of impact making the mass semi-mobile. Although shock-melted grains were not detected in V9, melted and contorted grains, principally quartz and pyroxene, are common, mostly confined to cracks that are possibly a result of cone vectors produced by the descending cloud forcing melted material deeper into the rind. The EDS spectrum (Fig. 7b) indicates high concentrations of quartz along with Al + Cl, the latter probably being Cl-rich Al + Si glass, which is probably a cosmic impact signature (Stebbins & Du 2002).

Additional supporting evidence for cosmic impact debris comes from the disrupted brecciated area (Fig. 7c) in the outer V9 rinds and from partially melted quartz and zircon. Because both minerals are of small dimension (*c.* 2 μm) they may possibly be

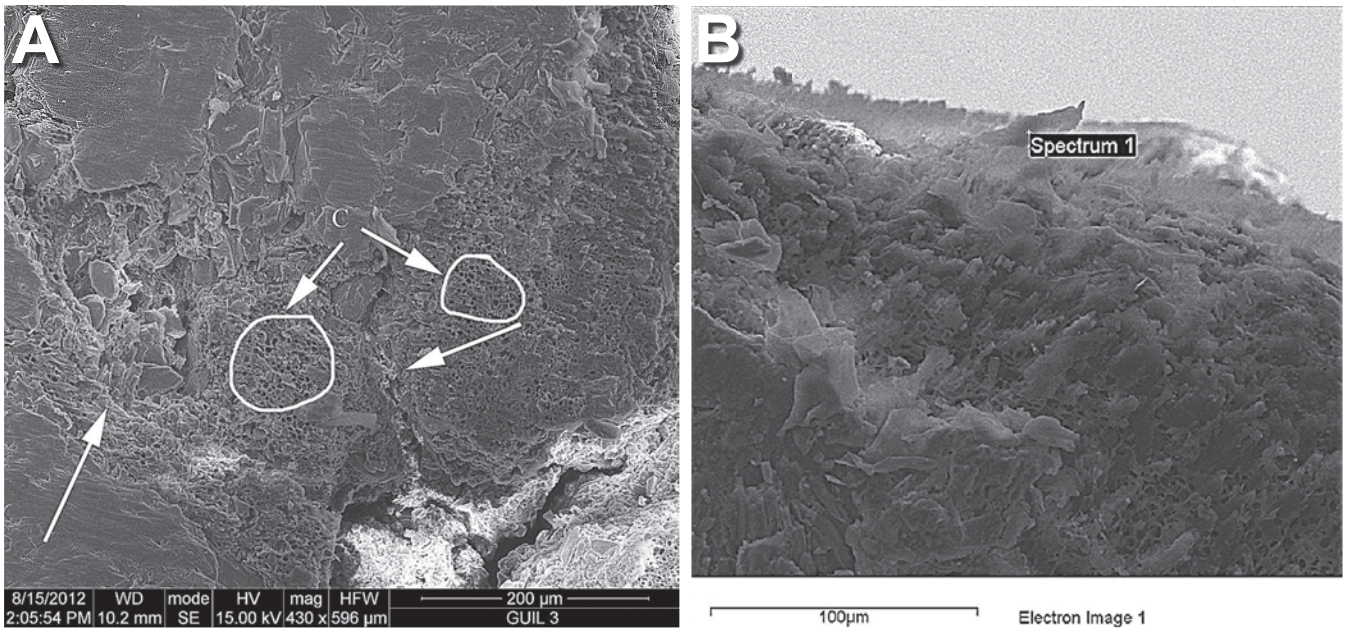

Fig. 5. (**a**) Transect from outer weathered zone of G3 inward toward the fresh lithic core. Melted quartz, zircon, olivine, pyroxene and Ca-plagioclase are common in groups (low centre and right of centre marked with arrows). Opaque carbon clusters circled. (**b**) Higher resolution image of breccia zone in the outer rind. Spot EDS spectrum shows C dominant with minor Na, Cl, K and O.

the result of long-distance transport from the impact or generated from a local airburst. Alternatively, they may be fused particles, with quartz being resident in the country rock and zircon incorporated in the descending cosmic cloud. The EDS spectrum (Fig. 7d) shows that zircon is dominant. Apart from zircon as an anomalous mineral in the rind, neighbouring elements in the breccia area of V9 (Fig. 8a–d) include Bi and Tc, both candidates confirming a possible cosmic influence, although the Tc may derive from atomic bomb testing or Chernobyl. The Bi, in particular, contains several isotopes linked to cosmic impacts (Brownlee 1985; Courty & Fedoroff 2010), being three times more common in meteorites than in the Earth's crust. Although isotopic data are lacking, the presence of both metals is suggestive of an impact origin, and Tc, in particular, as a transition metal, strongly suggests the presence, although unconfirmed at present, of small concentrations of Ir and possibly other platinum metals. A similar heavily brecciated area (Fig. 8c), on the same grain as shown in Figure 8a, carries C and Cr (EDS, Fig. 8d), which are probably products of wildfire and ablation from a cosmic cloud, respectively. The lack of Ca and minimal Al shown in Figure 8d may also suggest, not a mineral, but a non-stoichiometric melt.

The palaeosols

The palaeosols (Fig. 4) in both the LG moraine (G3) and the Traversette rockfall (V9) are nearly identical despite the very different sediment comprising resident parent materials (moraine comprising both till and glaciofluvial sediment, and rockfall made up of coarse clast-supported matrix material). Both palaeosols have similar depths (50 cm in G3 and 60 cm in V9); the latter formed over an open network of coarse material, with the former containing sufficient matrix material for analysis of the parent material to be undertaken. Both Ah and Bw horizons are thicker in G3 than in V9 and root penetration differs, with deeper extension in G3. Soil colours are closely similar in the upper horizons of the two profiles. The 10YR 2/3 colour indicating brownish black material in the surface epipedons is presumably close to the dynamic equilibrium of organic carbon for the environment.

Field textures begin with pebbly sandy loam material in the Cu and Cox horizons, somewhat more coarse in G3 than in V9. Upward in both profiles the texture remains similar to the C horizon in V9 but becomes pebbly silty loam in G3, remaining similar into the surface horizon. The texture in the Ah horizon of V9 is similar to that in G3, the silt content suggesting appreciable input of aeolian sediment, possibly corroborated by allochthonous quartz incorporated in the rinds.

Soil structure grades from granular in the Ah horizons of both profiles to weak blocky in the Bw horizons, becoming massive or structureless in the C horizons. As expected, moist consistence, which is very friable in the Ah of G3 and friable in V9, becomes friable in the Bw of G3 and very friable in V9. These variations in consistence reflect relatively small particle size variations. A variation of particle size within the C group of horizons, reflecting the different origins of the two profiles, leads to very friable consistence in V9 and loose consistence in G3, the latter being related to an increase in glaciofluvial sediment with depth in the profile. Stickiness mirrors textural changes, with G3 ranging from nonsticky to slightly sticky from the Ah to Bw horizon, and becoming nonsticky in the C group. In V9, stickiness ranges from zero in the Ah to slightly sticky down profile. Plasticity follows a similar pattern, with values of zero in all horizons.

Particle size

Particle size variations (Table 1) down profile mirror the field textures, with the greatest variations of sand in the G3 profile reflecting the glaciofluvial origin of the sediment in the lower horizons. Silt increases in the upper horizons of the G3 profile, presumably reflecting glacial grinding and aeolian influx, whereas, in contrast, the V9 profile exhibits an increase down profile suggestive of basal grinding during emplacement by mass wasting. Beyond that, clay content is minimal at <3%, which explains the lack of plasticity, slight stickiness and weak soil structure.

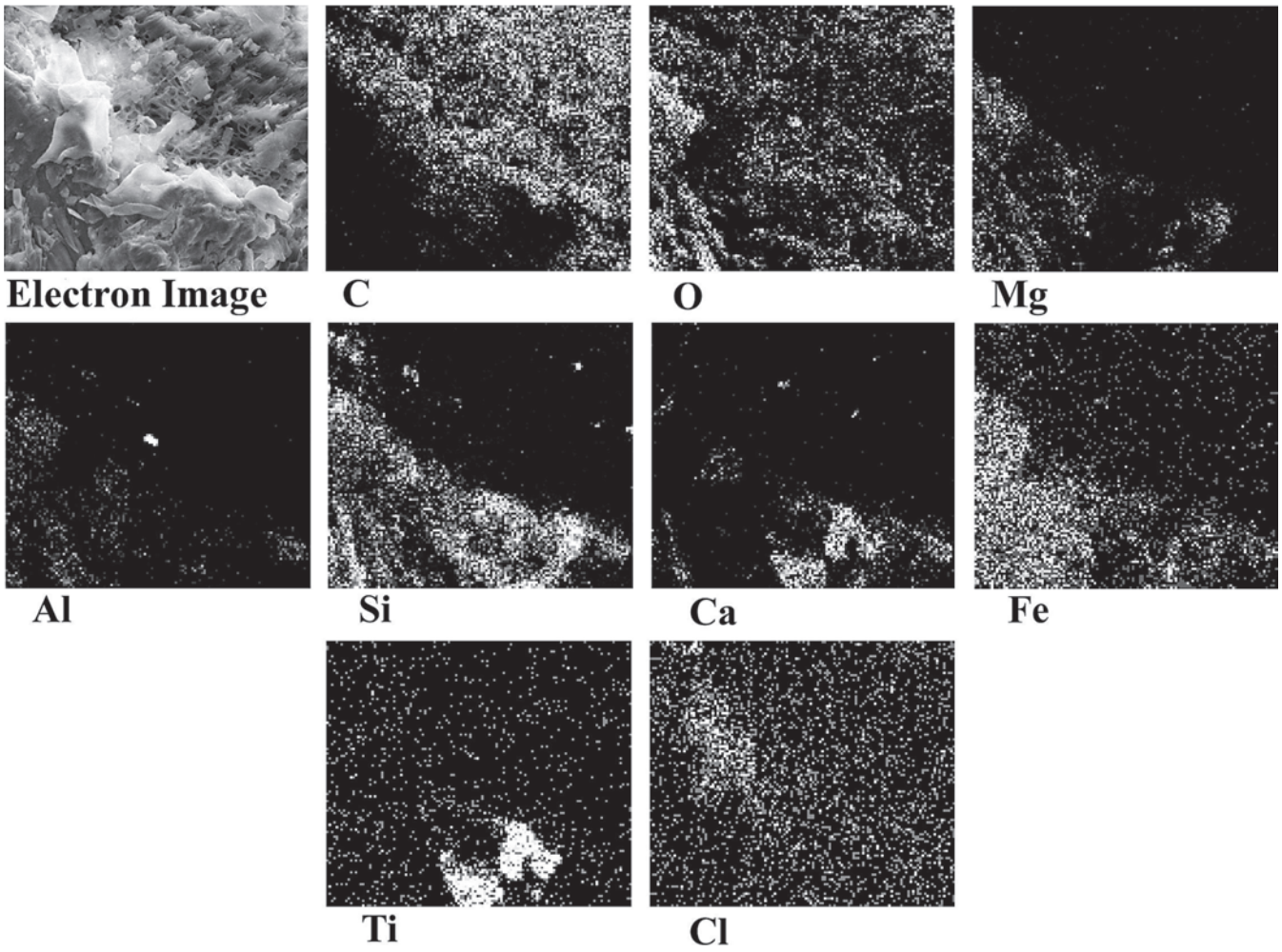

Fig. 6. G3 outer weathering zone chemical element map showing breccia in upper part with partially melted and shock melted pyroxene, Ca-plagioclase and quartz. The carbon-coated material is stronger to the upper right and less so to the lower right, where twisted and contorted pyroxene emit a strong spectral signature. The Si distribution follows melted/contorted quartz filling a rind fissure oriented from upper left to lower right in the SE image.

Mineralogy

Primary and clay mineral distributions of the clay fraction were analysed to determine weathering trends in the palaeosols. In both soils clay mineral content is dominated by chlorite and kaolinite (Table 2). The chlorite content varies in the G3 profile from 58.2 to 88.3% and in V9 from 46.0 to 59.8%. The kaolinite content remains between 7.6 and 39.6% in G3 and between 22.0 and 29.5% in the V9 profile, where it is more uniform. The main difference between the two profiles is the content of mica + illite; in V9 these minerals form 14.9–19.0% of the clay fraction, but in G3 they are found in trace amounts only (less than 1%). All samples contain small amounts of amphibole, and in some cases illite–vermiculite, talc and/or smectite are present. The mineralogy reflects overall the lithological variations in the Guil and Viso drainages, dominated by metabasalt (G3) and mica or amphibolite schist (V9), respectively.

Soil chemistry

The pH and total salt content (Table 3) of the two profiles are somewhat similar despite differences in lithology. Both the G3 and V9 profiles contain strongly acid Ah horizons grading downward into Bw horizons of similar reaction (G3) or become very strongly acidic (V9). Thereafter in the Cox/Cu horizons, pH either rises to moderate acidity (G3) or becomes strongly acidic (V9). Total salts, estimated by electrical conductivity, are probably determined by nitrate content dictated by plant species variations. Total salts are highest in V9, with most salt content confined to the Ah/Bw group of horizons. The G3 profile trend shows slightly higher values in the Ah horizon decreasing with depth. Although not conclusive proof of an extraterrestrial (ET) anomaly, the selected chemical elemental composition shows anomalously high percentages of specific elements compared with mean crustal compositions (Rudnick & Gao 2005). The anomalous geochemistry may result from the air-influx of terrestrial impact ejecta from elsewhere. Compared with the lack of ET specific chemistries in the Cretaceous–Palaeogene impact of 65 Ma, it is not surprising that the G3 site lacks a conclusive ET imprint (Huber & Koeberl 2012).

Palaeosol microscopy

Residual sands in the Ah horizon of the G3 palaeosol reveal a combination of contorted, brecciated and melted mineral grains with chemistries similar to those of black mat weathered sediment in

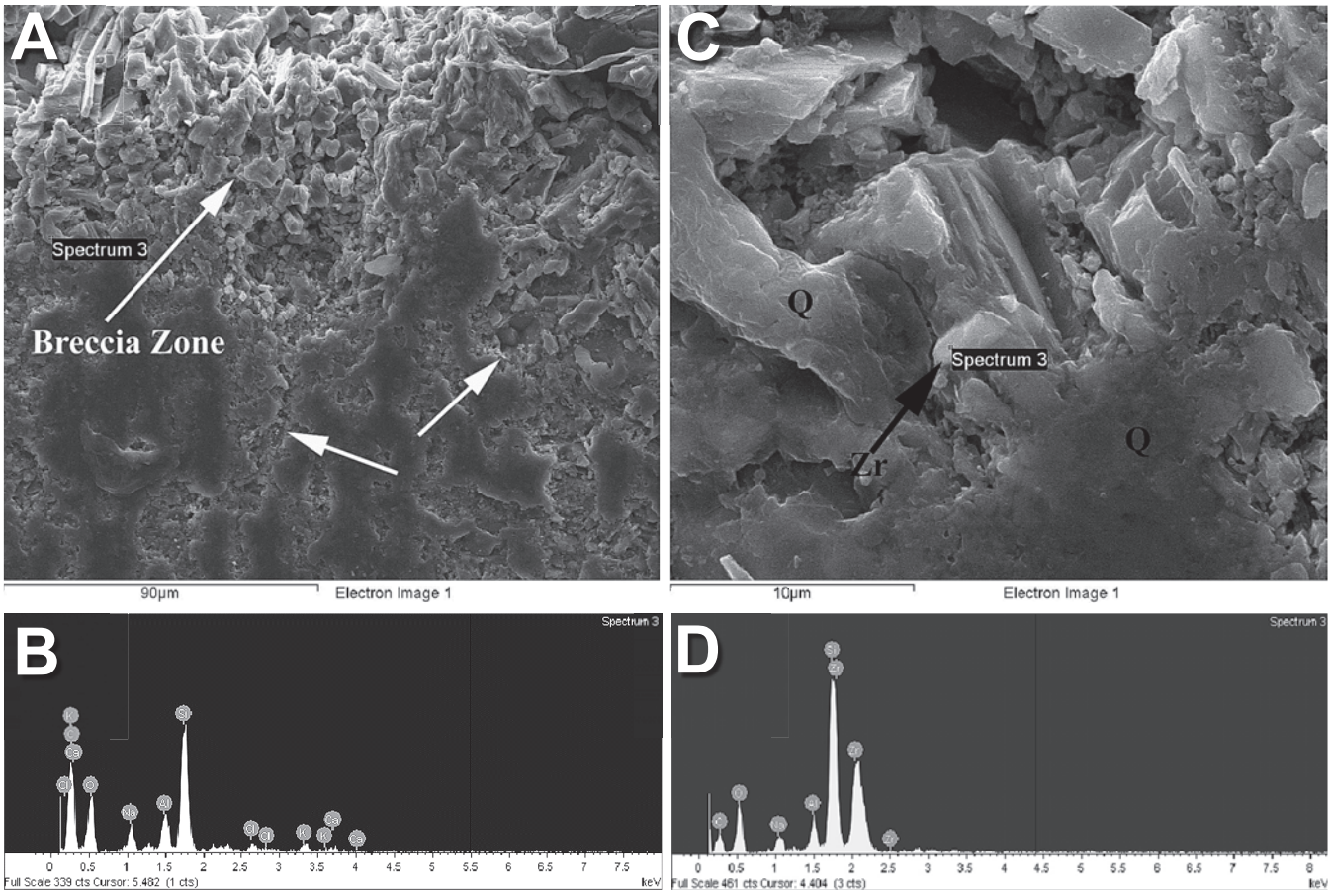

Fig. 7. (**a**) Image of outer (breccia zone) and mid-section of the V9 rind with prominent cracks filled with melted material (arrows) presumably partially fluidized during impact. (**b**) EDS spectrum showing Si with cosmic Al + Cl and high concentration of carbon on quartz. (**c**) Disrupted brecciated outer rind area of V9 with partially melted quartz and zircon. (**d**) EDS spectrum showing primarily zircon and minor C.

other parts of the world. Grains subjected to extreme impact produce brecciated surfaces similar to what is illustrated in Figure 9a, which provides an example of welded materials. In this case, the main grain is a pyroxene of fine sand grade size welded to spinel. The high Mn concentration (Fig. 9b) in the spinel may well be in nodular form although nodules were not imaged.

Other pyroxene grains exhibit less breccia and surface melting but carry considerable carbon welded to the grain surface as shown in Figure 9c. The high number of adhering particles may be related to glaciation and glacial grinding; the finer among them may also be related to the descending black mat cloud that affected the deposits. The EDS spectrum in Figure 9d shows a chemistry suggesting augite as the mineral. Other pyroxene grains carry very thick and opaque carbon mats (Fig. 10a), which warrant more detailed analysis to determine if they contain the common glassy carbon spherules often found in black mat sediments (Mahaney *et al.* 2010). The extreme melting of the surface quartz grain, shown in Figure 10b, appears welded onto another grain below.

Palaeosol microbiology

To determine the metagenomic similarity between G3 and V9 profiles or horizons and other palaeosols in the French–Italian palaeosol or soil sequence we analysed their eubacterial populations. Comparisons were made between the Ah, Bw, Cox and Cu (where present) horizon eubacterial populations using DGGE analysis of 16S rRNA genes isolated from the bacterial community in the sediment collected from various sample sites. Initial comparisons were made between the Cox and Bw horizons (data not shown), and Ah and Bw horizons in the Guil valley samples (Fig. 11a). These comparisons indicate that the Ah and Bw microbial populations in the G1 and G2 soils (YD moraines) are similar to each other. However, the bacterial population in the G3 Ah is dissimilar to that found in the other two adjacent sample sites (G1 and G2), and also in the G3 Bw horizon (Fig. 11a). It would be premature to say that this reflects an effect associated with the black mat event (as the G1 and G2 palaeosols were deposited after the event), but the result merits further microbial analysis to test this hypothesis.

A comparison of the eubacteria found in the Bw horizons of the Guil and Viso valley palaeosols (six sample horizons in total) is shown in Figure 11b. These data suggest the following: (1) Bw populations in the two regions (Guil and Viso) are distinct, the Guil samples especially forming a cluster; (2) the atypical G3 Ah eubacterial composition and the black mat affected rind on the palaeosol surface, when considered together, strongly suggest an anomalous microbial ecological history that may have resulted from intense heat, radiation and trace mineral deposition induced by a cosmic airburst.

Discussion

Mean maximum rind thicknesses reported here are comparable with thicknesses reported elsewhere from much shorter time since

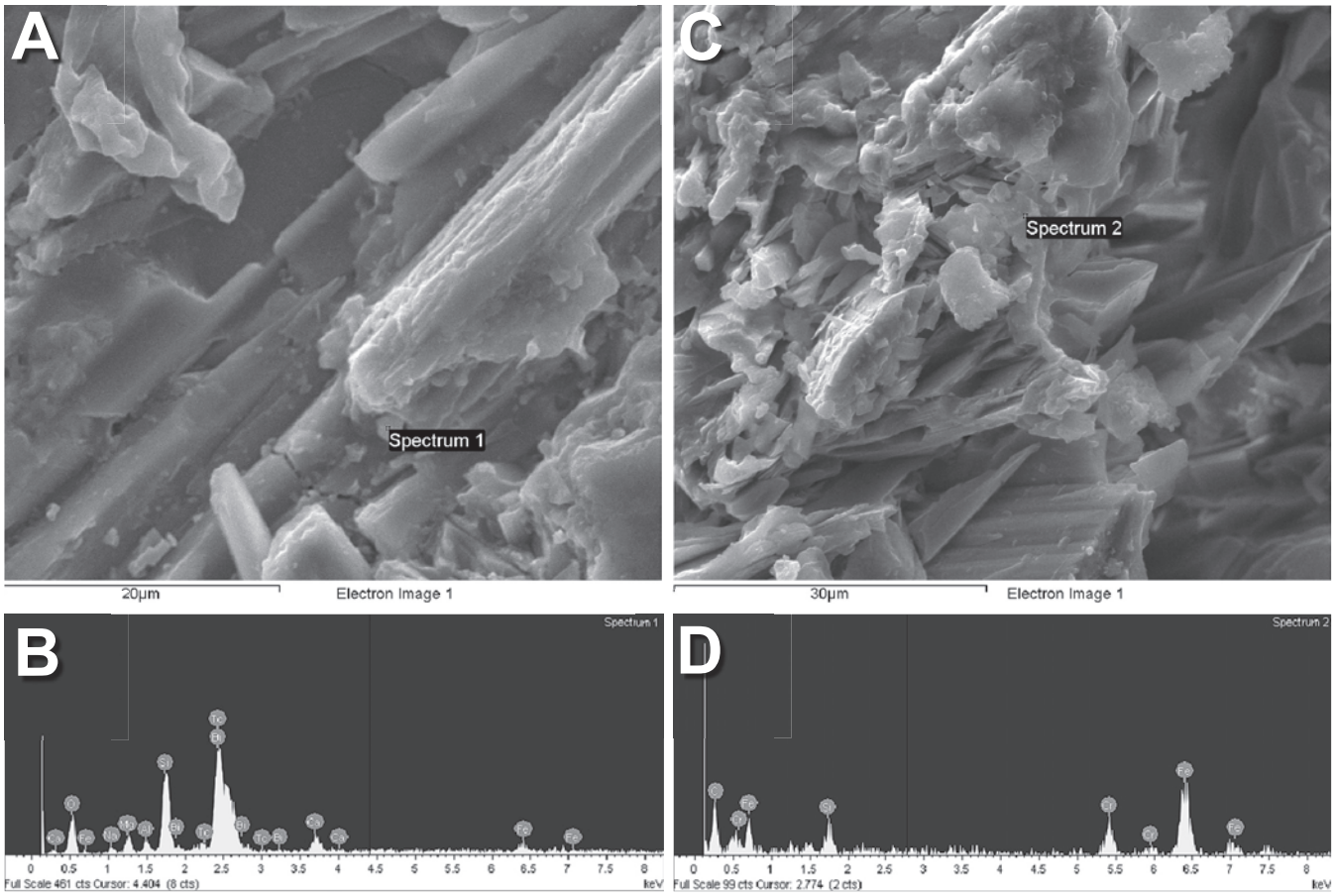

Fig. 8. Brecciated area of the outer rind of V9. (**a**) Image carrying a signature of Bi and Tc; the latter transition element is a cosmic impact signature. (**b**) EDS spectrum. (**c**) Image of a brecciated suface on the same hornblende grain carrying a Cr coating. The lack of Ca and minimal Al may suggest a non-stoichiometric melt. (**d**) EDS spectrum.

Table 1. *Particle size distributions in Late Glacial palaeosols, Western Alps*

Horizon	Depth (cm)	Sand %	Silt %	Clay %	Mean φ*
Site GUIL3					
Ah	0–16	52.4	45.2	2.4	3.3
Bw	16–32	34.8	63.0	2.2	4.6
Cox	32–45	53.8	45.0	1.2	3.3
Cu	≥45	72.2	27.5	0.3	2.2
Site VISO9					
Ah	0–12	64.5	32.5	3.0	3.1
Bw	12–22	54.9	44.1	1.0	3.5
Cox	22–60	52.9	44.1	3.0	3.5

*Mean φ = Σ(25th + 50th + 75th %)/3.
Particle sizes: sand 2000–63 µm; silt 63–2 µm; clay <2 µm.

deposition, particularly those reported by Nicholson (2008) in southern Norway, André (1996) in northern Sweden and Etienne (2002) in Iceland. Assuming those workers did not measure fracture faces that weather inordinately fast, the reported differences may well reflect different microenvironments, lithological differences or loss by erosion (Mahaney *et al.* 2012*a*). As noted by Etienne (2002) in his model of cyclic growth of rind behaviour, rinds may lose material by microerosion processes unless, as pointed out by Mahaney *et al.* (2012*a*), they become armoured by an Fe-skin at surface. The growth of such armoured specimens depends almost entirely on the redox potential at the clast surface, and the speed and degree of armouring (Fe^{3+} cementation), which controls porosity and invasion of fluids. Given the Late Glacial age of rinds reported here and the 'armouring effect' achieved by extreme melting on impact early in their weathering history, it is likely that the mean values are an approximate measure of weathering since time zero (deposition in stillstand recessional moraines, *c.* 13–15 ka). Other researchers (Gordon 2005; Gordon & Dorn 2005) have pointed to microerosion processes as reducing rind thickness over time; when these processes are gauged against cosmogenic accumulation dates (where available), it is considered that (rind) thickness may present minimum ages since deposition, a subject fully discussed by Mahaney *et al.* (2012*a*). Because rind measurements are usually presented as mean values it could be that plus and minus values measured in a standard population relate to armoured v. unarmoured clasts, the latter presenting prime exfoliation candidates. In particular, Gordon (2005) showed how Si glaze sealed pores in basalt rinds, thus generating an armouring effect, similar to redox-fluxed rind surfaces releasing high concentrations of Fe^{3+} (Mahaney *et al.* 2012*a*,*b*).

The black mat bed, normally a 2–3 cm thick encrustation of C + Fe + Mn on pebbly sand of felsic gneiss and granitic composition, together with glassy carbon spherules, as found in the Andes (Mahaney *et al.* 2008) is missing in the Guil valley of France and the Upper Po valley of Italy. As shown with the Andean example, the burnt layer material represented by a high-carbon signature was

Table 2. *Mineralogy of the <2 μm fraction of two Late Glacial palaeosols, Mt. Viso area, France–Italy*

Sample	Chlorite %	Illite–vermiculite %	Mica + illite %	Kaolinite %	Talc %	Smectite %
Guil3-Ah	58.2	2.3	tr.	39.6	0.0	0.0
Guil3-Bw	86.7	tr.	tr.	12.9	0.0	0.0
Guil3-Cox	88.3	1.0	tr.	7.6	3.1	0.0
Guil3-Cu	71.6	tr.	tr.	14.2	5.4	8.3
Viso9-Ah	54.7	0.0	14.9	29.5	0.9	0.0
Viso9-Bw	59.8	0.0	17.3	22.0	0.9	0.0
Viso9-Cox	46.0	10.1	19.0	24.0	1.0	0.0

tr., trace.

Table 3. *Selected chemical parameters* for the G3 and V9 profiles*

Horizon	Depth (cm)	EC (S cm^{-2})	pH (1:5)	Co	Cr	Cu	Ni	Sc	V	Th
Site G3										
Ah	0–16	9.1	5.4	43	424	66	163	33.3	235	3.5
Bw	16–32	7.4	5.3	50	374	74	207	41.3	276	2.3
Cox	32–45	5.6	5.7	60	364	95	241	39.1	263	1.1
Cu	≥45	4.7	5.7	63	350	117	402	36.9	279	<0.5
Site V9										
Ah	0–12	41.0	5.4	–	–	–	–	–	–	–
Bw	12–22	26.1	4.9	–	–	–	–	–	–	–
Cox	22–60	4.9	5.1	–	–	–	–	–	–	–
Crust†				15.6	73.5	23.2	35.1	11.7	79.0	0.4

*Elemental data in ppm.
†Data from Rudnick & Gao (2005)
EC, electrical conductivity.

first thought to result from a lightning strike and resultant fire, although the conflagration temperature in a wet tundra undergoing first- or second-stage succession vegetation growth would not be high. Admittedly, brushfire temperatures are certainly not high enough to produce glassy C-rich spherules firmly welded to mineral surfaces as in the Andean example (Mahaney *et al.* 2010, 2011*a,b*). Despite the missing black mat bed in the Alps, the rind archive of associated carbon welded onto pyroxene and quartz, dislocated and partially melted and shocked pyroxene and quartz species together with brecciated mineral grain surfaces, presumably resulting from impact, leads to a testable hypothesis more in line with previously reported data (Mahaney *et al.* 2011*a*,*b*). The high-carbon layer in the rind material of the Alps is similar to burnt material correlated by Mahaney *et al.* (2010) with the black mat beds described elsewhere in North and South America, Europe and Central Asia.

The analysis of cosmic-affected grains in two palaeosols under discussion here requires a comparison with previous long-distance transport of the black mat described in the Northern Andes (Mahaney *et al.* 2008, 2010). Specific grain microtextures include intense brecciation and internal fracture patterns in both sample suites, with the degree of brecciation being of similar intensity in both the Andean and Alps samples. Brecciation may be a function of both impact and heating, with incoming high-speed particulate matter releasing enormous kinetic energy capable of producing disruption of mineral fabric to a rind depth of 1000 μm, and crack propagation reaching deeper into the rind bodies. Microfractures are oriented, both parallel and normal to the surface, the pattern being related to variable impact energy and resulting energy cone vectors. Microfractures reported here are similar to those in Andean samples analysed by Mahaney *et al.* (2011*b*).

The microbiology DGGE analysis of the horizons in profiles G3 and V9 suggests that minor eubacterial differences between these palaeosol horizons could be linked to the proposed black mat event. As shown in Figure 11a, the Ah horizon in G3 shows a different DGGE pattern from other analysed Ah and Bw horizons in the Guil valley sample sites (Fig. 11b). This figure shows that the distance value of the line represented by G3 is greater than for any other community studied in the DGGE image. It also appears in a separate branch of the dendrogram to the other clustered samples analysed (G1A, G1B, G2A, G2B, G3B), indicating the population of bacteria in this sample has greatest dissimilarity when compared to the other five samples. The meaning of this remains unclear until further analyses (such as pyrosequencing) are undertaken. Changes may be due to very minor bacterial nutrient differences in the pre- and post-black mat impact palaeosols. The V9 Ah horizon population was not compared with other Ah horizons in the Viso region. This is because our analysis of the Bw and Cox horizons in this region suggests much less similarity between the microbial populations in the Viso sample sites (Figs 11a,b).

One explanation for the G3 Ah DGGE result is that trace elements released into this palaeosol through the impact event could still be fixed within the Ah sediment matrix and could continue to have had a selective pressure on 13 kyr of microbial population development. We reached this conclusion for the following reasons: (1) the effect of trace elements, and even sources of radioactivity, on microbial growth is well established; (2) it is conceivable that, over many generations, the presence of different trace elements in a palaeosol microenvironment could have a noticeable effect on the structure of a stable microbial population; (3) it is still not fully understood why in any sediment environment such very wide microbial diversity is typically observed. This provocative black mat-microbe impact hypothesis deserves further testing. It should be noted that there are also more mundane explanations for the eubacterial differences in the G3 Ah horizon; for example, multiple repeat testing of soil samples in metagenomic analysis may be

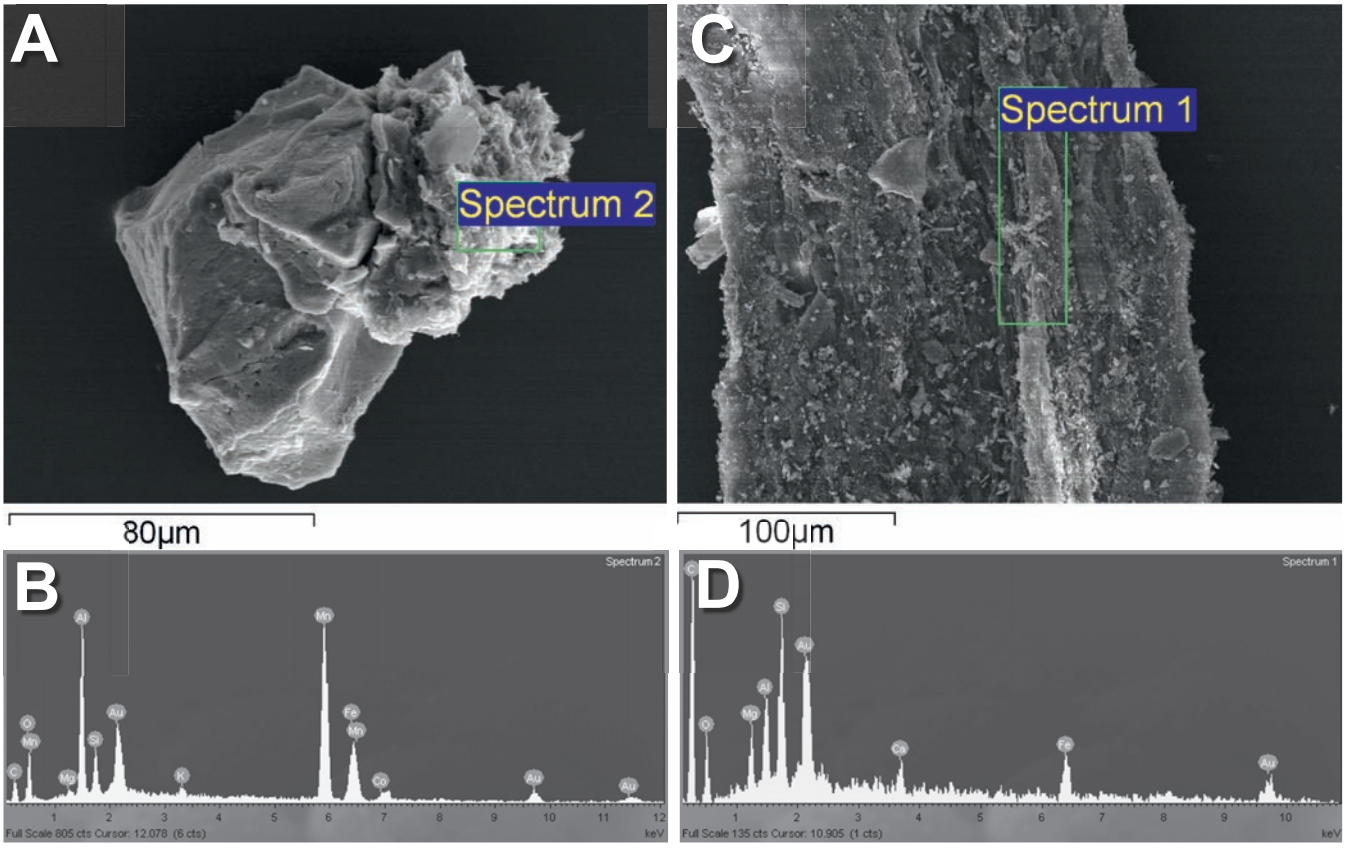

Fig. 9. (**a**) Angular spinel with brecciated surface and a carbon signature in the G3 Ah horizon. (**b**) EDS spectrum. The Mn may be a cosmic impact signature in micro-nodular form although no nodules were identified. (**c**) Probable augite with angular particles and carbon welded to the grain surface in the G3 Ah palaeosol horizon. (**d**) EDS spectrum showing expected higher Al and lower Ca than are present in other pyroxene species.

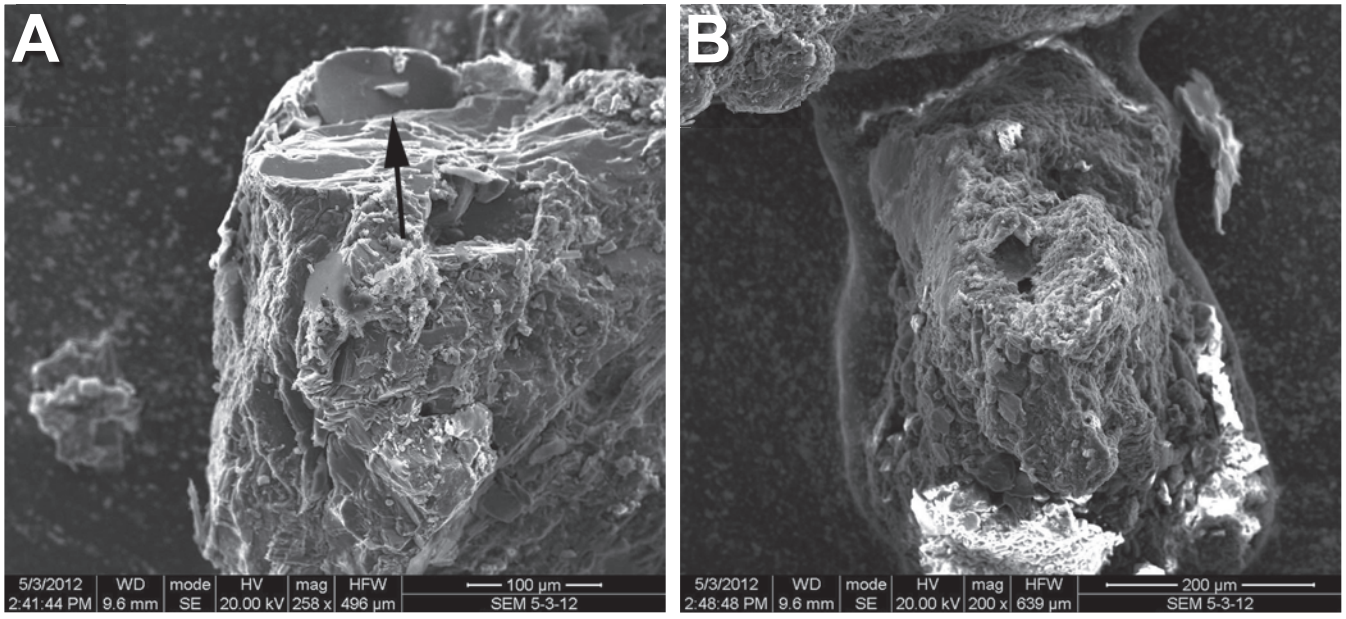

Fig. 10. (**a**) Disrupted and partially melted pyroxene with carbon (arrow) welded to surface. (**b**) Melted pyroxene in the palaeosol Ah horizon of the G3 profile.

necessary if variations in the microbial populations at the micro-scale are to be ruled out in such a small sample selection.

Microbiological differences between the Guil and Viso samples are apparent in the Bw horizons (Fig. 11b), but this is probably linked to the localized environment and different lithologies. Again, further information may be gained by more detailed 16S rRNA sequence pyrosequencing of these populations. It should be remembered that in a gram of sediment containing 10^8–10^9 bacterial cells

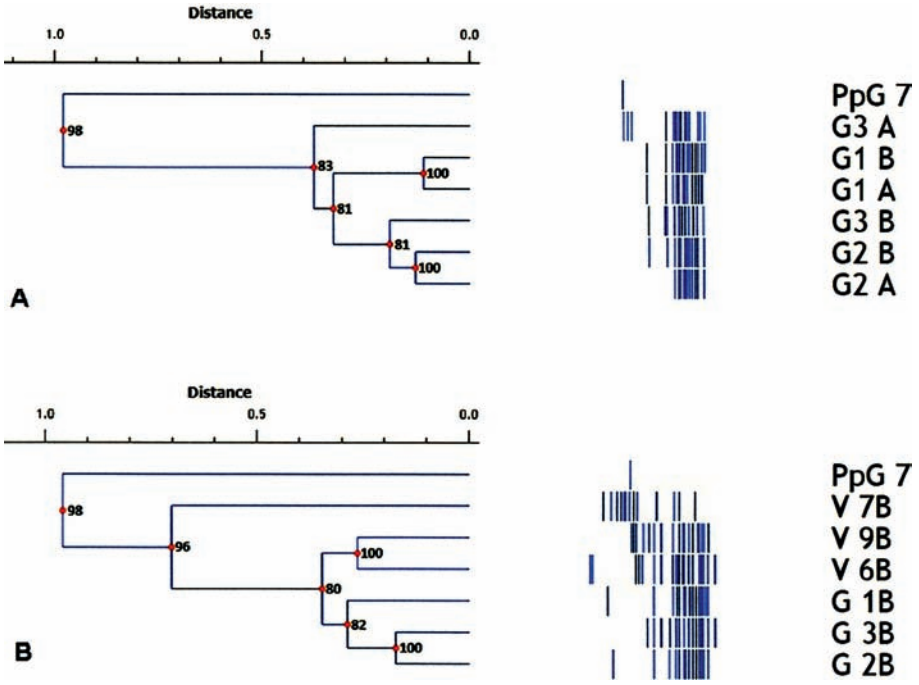

Fig. 11. (**a**) Comparison of eubacteria populations in Ah and Bw horizons taken from three palaeosols (G1, 2 and 3) located in the Guil valley. These data suggest that the G1 and G2 samples (YD) are characterized by very closely related Ah and Bw horizons. However, the G3 Ah horizon is clearly different and might be an anomaly related to the black mat impact. Pp G7 is a pure strain negative control, included for comparative purposes. (**b**) Comparison of eubacteria populations in Bw horizons taken from six palaeosols located in the Guil (G1-B–G3-B) and Viso (V6–9-B) valleys. These data suggest that the Guil valley samples form a closely related group. The V9-B and V6-B samples are also relatively similar. These findings might be expected given differences in microclimate and sediment geology from the moraine or rockfall deposits in the two locations. Experiments were duplicated with the same DNA to ensure reproducibility.

there will be $\geq 10^4$ different eubacteria and archaea genospecies (Schloss & Handelsmann 2006). Used as a phylogenetic tool to show how genetically similar specific species of bacteria may be, a 16S rRNA gene similarity of 95% is taken as an indicator that two organisms belong to the same bacterial species. However, even without further 16S rRNA analysis, our DGGE results certainly support a markedly different genospecies composition in the G3 sample when compared with analysis from adjacent sample sites. A clear conclusion of the DGGE studies is that the Ah, Bw, C/Cox and Cu horizon samples harbour differing microbial populations.

Black mat material reported in the Andean samples includes fibrous carbon-rich material carrying accessory Fe and Mn to glassy C-rich spherules, the latter often welded into grain surfaces, covered with layers of Fe and Mn and producing many twisted and contorted forms. Carbon sheets in the Andes are normally thick whereas in the Alps carbon may be exceedingly thin to opaque and thick, exceeding 1 μm, and welded to topographically irregular grain surfaces, often complexly intergrown in some cases. The Andean samples display brecciated microfeatures forming radial patterns extending into zones of high-frequency microfractures produced by particle impact or high-temperature soot release from wildfires, or heat release from an incandescent cloud. As observed, heat-induced microfractures are random in the Alps samples, and are widely spaced, exhibiting cracks wider than in the Andes. Compared with the black mat Andean samples, microfractures in the Alps samples are tightly packed into high-density areas that could be vibration generated, and the troughs are filled with shock-melted material, which may have been viscous streams shortly after impact that cooled rapidly thereafter.

Many crenulated or scalloped grains in the Andean sample group show thick C-coatings also containing some Al and Cl. The Al, scarce as it is in the local pyroxene-rich lithology, could be scavenged from other country rock minerals with the Cl related to aluminosilicate glasses that could have an interstellar origin (Stebbins & Du 2002). The occurrence here in V9 is similar to what has been previously reported by Mahaney *et al.* (2010).

The black mat Andean database, coupled with the Alps specimens reported here, thus far support a theory of kinetic energy release from mass impact of particles in an incandescent carbon-rich cloud. It is likely that particle impact and heat produced the commonly observed brecciated surfaces along with a high frequency of closely spaced microfractures and larger crack systems. To achieve brecciation may depend upon grain-to-grain collisions at extremely high velocity, although with variable masses involved. Incoming ejecta are expected to consist of very fine sand to silt particles; the resident coarse clastic pebble- and cobble-size material records the event, along with surface regolith in the initial stage of soil formation. Both surface coarse clasts and soil sediment received heat and particle impact, judging by the production of carbon encrustations, shock melted host grains in rinds and palaeosols, and propagation of micro- and macro-crack systems, the latter acting as conduits of semi-viscous material. The presence of welded C-bonded material argues for extreme heat release at temperatures higher than 900 °C, apparently high enough to melt pyroxene, but possibly not high enough to totally melt quartz. Because the exact temperature of incoming ejecta is unknown, the temperature necessary to weld carbon to grains without melting quartz would lie somewhere between 900 and 1670 °C (melting temperature of quartz is 1713 °C, if β tridymite and cristobolite are present (Deer *et al.* 1966; Frondel 1962)). The presence of low-temperature Bi suggests either a local or a cosmic origin, but actual proof requires that isotopes be worked out in future.

Possible alternative hypotheses to explain black mat sediment focus on the nature of the rinds or palaeosols where the impact material resides, which are all in surface exposures, in contrast to the Andean site (Mahaney *et al.* 2008) where the black mat resides in glaciolacustrine sediment buried under an outwash fan. The flux of water and organic compounds in the Andean aquifer produces chemilithotrophic bacteria (Bougerd & De Vrind 1987), as well as alternating redox conditions favouring retention of C, Mn and Fe. The Andean alternative hypothesis parallels that of Quade *et al.* (1998), who argued that the black mat is the product of subsurface drainage

accumulation of organic and associated oxides and hydroxides, with no evidence of a cosmic connection. Because bacteria in the Alps appear to be absent in the rinds but present in the palaeosols, it would seem that alternating redox conditions apply only in the palaeosol. Arguing against a terrestrial origin, a null hypothesis includes the high frequency of brecciation, thick carbon encrustations mostly intertwined with minerals, extensive microfractures and wider cracks propagated inward toward a fresh lithic core, and partial to full shock-melted grains. These are certainly not manifestations of normal terrestrial processes. We did not search for nanodiamonds, planar deformation features, and Ir/Os, and their lack softens the cosmic hypothesis, but with a distance of >5000 km between the primary impact site in southern Canada and the terminal zone of the ejecta in the Alps, the question of dispersal of impact material is still open. The breakup in space of a comet or asteroid prior to impact could produce a surface or oceanic impact by the largest object, and hundreds of smaller fragments could create airbursts affecting an entire hemisphere (Bunch *et al.* 2012). Approximately 90% of all ejecta from the main impact would fall within five crater radii, although fine material is expected to be randomly distributed over a much larger area. Although the type of impact vehicle is still uncertain, the present theory (Napier 2010) is that a fragmented comet produced multiple impacts or airbursts over at least 10% of Earth, releasing an estimated 10×10^6 tonnes of Fe spherules (Wittke *et al.* 2013).

A second alternative hypothesis might question the lack of both C-rich spherules and chondrules as important evidence arguing against a cosmic origin. Comparison of the C-rich spherules in the Andean black mat with similar samples analysed by Firestone *et al.* (2007) shows more similarities than differences. Although no carbon-rich spherules have been identified in the Alps rind samples thus far, it is likely that there was too little local vegetation to produce them, as they are reported to be produced by incineration of tree sap (Firestone *et al.* 2007). Additional analysis may yet reveal the presence of microspherules that would help to bolster a cosmic origin.

A third alternative hypothesis could be mounted that the fired rock underwent extremes of heat without the necessity for an impact. However, although low- and high-temperature firing experiments have produced microfractures around grain edges of quartz, producing a micro-brecciated effect, the experiments could not reproduce the fusion of carbon with quartz. Moreover, the twisted or contorted and melted nature of selected grains in both the Andean black mat and the Alps samples requires a higher energy than could result from a low-grade bush fire or higher-grade lightning strike. After considering the partial evidence presented here, a cosmic connection offers the best explanation.

Future investigations in other catchments might reveal geomorphological and stratigraphic information related to an airburst, all of which might build on the database presented here, documenting a resurgence of ice following the breakup and retreat of glaciers in the Late Glacial. Ice overran older Late Glacial moraines consisting of till and glaciofluvial sediment, which can be dated using relative age criteria.

As an underappreciated palaeoenvironmental archive, weathering rinds in the Alps discussed herein and elsewhere (Mahaney *et al.* 2012*a*,*b*, 2013*a*; Mahaney & Keiser 2013) are now known to contain a wealth of mineral, chemical and biotic materials that record environmental change and genesis of alteration products over exceedingly long periods of time. On Earth, this time span may be limited to the last glaciation as discussed here, to the Early Pleistocene in the tropical mountains (Mahaney *et al.* 2012*a*, 2013*b*), or to the Miocene or slightly older in Antarctica, but on Mars, as shown by Fairén *et al.* (2011) and Mahaney *et al.* (2012*b*), this time span may extend from the earliest epoch (Early Noachian, *c*. 4 Ga) to the present. Moreover, the relation between weathered rinds in surface clasts and resident soils or palaeosols correlated with them on both Earth and Mars deserves more refined analysis in future. Considering what is known of terrestrial rinds, both from the Alps and Antarctica, and those from Mars (Fairén *et al.* 2011; Mahaney *et al.* 2012*b*), continued sampling of surface clasts and associated palaeosols suggests that there is every expectation of uncovering detailed palaeoenvironmental archives.

Conclusions

Normal relative age determinations of Late Glacial moraines and rockfall in the Western Alps of France and Italy led to detailed analysis of single weathering rinds in clasts of metabasalt, yielding evidence of cosmic impact archived within the weathered surface. High-resolution analysis of the rind material by SEM–EDS led to the identification of contorted grains of resident minerals that were melted at >1600 °C, thin to thick sheets of carbon welded to grain surfaces, brecciated surface material and the presence of Tc, a transition metal to platinum. The data indicate that the impact occurred in wet tundra when an early seral stage of vegetative development and soil morphogenesis was inundated by a high-temperature, carbon-rich cloud with a temperature at or very near the melting temperature of quartz. Although certain cosmic impact characteristics common at other impact sites are not yet evident here, the available evidence suggests that the rinds are equivalent to black mat beds seen elsewhere, and contain archived palaeoenvironmental information related to the YDB and onset of the YD glaciation. The microbiology results presented here also tentatively point to differences between the LG and YD Ah horizons that could be related to the proposed impact event. Because absolute ages for both the LG and YD moraines are lacking, future investigations ought to centre on establishment of absolute age controls for the moraine surfaces.

What is most remarkable, and as demonstrated herein, is that weathering zones in clast rinds are a microcosm replicate of weathering zones (horizons) in associated palaeosols forming in deposits. The data show that clast weathering produces near-similar weathering effects and products compared with resident palaeosols of the same age and similar lithology. Correlation of clast rind weathered products with palaeosol morphology has not previously been seen by workers who have used rinds to provide relative ages on glacial and periglacial deposits. Recent palaeosol stratigraphy of Plio-Pleistocene deposits in the tropical alpine environment of Mt. Kenya (Mahaney *et al.* 2013*b*), coupled with clast rind analysis of similar-age deposits in the same area (Mahaney *et al.* 2012*a*), suggests that there exists considerable scope to increase recovered palaeoenvironmental archive information by combining rind and palaeosol analyses. In certain circumstances, these analyses may be extended into the Palaeogene and possibly beyond.

Because weathering rinds appear to provide prolific information about terrestrial palaeoenvironments, with chemical and biotic alterations recording intricate details in atomic space over partial and whole periods of geological time, it is likely that the pursuit of rind and palaeosol analyses in the Antarctic and on Mars would yield fruitful results. Given the time span for rind development on Mars, it is also likely that asteroid and comet airbursts and impacts might be recorded in clast rinds in situations similar to the evidence from the Alps discussed here.

This research was funded by Quaternary Surveys, Toronto, and the QUESTOR Centre (studentship to P. Pentlavalli). We are indebted to D. Nicholson (Manchester Metropolitan University) and R. Dorn (Arizona State University) for critical reviews and insightful comment that greatly improved the paper.

References

André, M.-F. 1996. Rock weathering rates in Arctic and subarctic environments (Abisco Mountains, Swedish Lappland). *Zeitschrift für Geomorphologie*, **40**, 499–517.

Ashley, J.W., Golombek, M.P., *et al.* 2011. Evidence for mechanical and chemical alteration of iron–nickel meteorites on Mars—process insights for Meridiani Planum. *Journal of Geophysical Research*, **116**, doi:10.1029/2010JE003672.

Birkeland, P.W. 1973. Use of relative age dating methods in a stratigraphic study of rock glacier deposits, Mt. Sopris, Colorado. *Arctic and Alpine Research*, **5**, 401–416.

Birkeland, P.W. 1999. *Soils and Geomorphology*. Oxford University Press, Oxford.

Bougerd, F.C. & Devrind, J.M.P. 1987. Manganese oxidation by *Leptothrix discophora*. *Journal of Bacteriology*, **169**, 489–494.

Broecker, W.S., Denton, G.H., Edwards, R.L., Cheng, H., Alley, R.B. & Putnam, A.E. 2010. Putting the Younger Dryas cold event into context. *Quaternary Science Reviews*, **29**, 1078–1081.

Brownlee, D.E. 1985. Cosmic dust: collection and research. *Annual Review of Earth and Planetary Sciences*, **13**, 147–173.

Bunch, T.E., Hermes, R.E., *et al.* 2012. Very high temperature impact melt products as evidence for cosmic airbursts and impacts 12,900 years ago. *Proceedings of the National Academy of Sciences of the USA*, doi/10.1073/pnas.1204453109.

Canada Soil Survey Committee. 1977. *Soils of Canada 1*. Agriculture Canada, Ottawa, ON.

Chinn, T.J. 1981. Use of weathering rind thickness for Holocene absolute age-dating in New Zealand. *Arctic and Alpine Research*, **13**, 33–45.

Courty, M.-A. & Fedoroff, M. 2010. Soil morphologic indicators of environmental hazards linked to cosmic airburst. 19th World Congress of Soil Science, Soil Solutions for a Changing World, 1–6 August 2010, Brisbane (DVD).

Day, P.E. 1965. Particle fractionation and particle size analysis. *In*: Black, C.A. (ed.) *Methods of Soil Analysis*. American Society of Agronomy, Madison, WI, 545–567.

Deer, W.A., Howie, R.A. & Zussman, J. 1966. *An Introduction to the Rock Forming Minerals*. Longman, Harlow, 340–355.

Dixon, J.C., Thorn, C.E., Darmody, R.G. & Campbell, S.W. 2002. Weathering rinds and rock coatings from an Arctic alpine environment, northern Scandinavia. *Geological Society of America Bulletin*, **114**, 226–238.

Dorn, R.I. 2009. Desert rock coatings. *In*: Parsons, A.J. & Abrahams, A.D. (eds) *Geomorphology of Desert Environments*, 2nd edn. Springer, Berlin, 153–186.

Etienne, S. 2002. The role of biological weathering in periglacial areas: A study of weathering rinds in south Iceland. *Geomorphology*, **47**, 75–86.

Fairén, A.G., Dohm, J.M., *et al.* 2011. Meteorites at Meridiani Planum provide evidence for significant amounts of surface and near-surface water on early Mars. *Meteoritics and Planetary Science*, **46**, 1832–1841.

Firestone, R.B., West, A., *et al.* 2007. Evidence for an extraterrestrial impact 12,900 years ago that contributed to the megafaunal extinctions and the Younger Dryas cooling. *Proceedings of the National Academy of Sciences of the USA*, **104**, 16016–16021.

Frondel, C. 1962. *Dana's System of Mineralogy,Volume II. Silica Minerals*. Wiley, New York.

Ge, T., Courty, M.M & Guichard, F. 2009. Field-analytical approach of land–sea records elucidating the Younger Dryas syndrome. *American Geophysical Union Fall Meeting*, Abstract PP31D-432, 1390.

Gibbard, P.L. 2004. Quaternary … now you see it, now you don't. *Quaternary Perspectives*, **14**, 89–91.

Gordon, S. 2005. Localized weathering: Implications for theoretical studies. *Professional Geographer*, **57**, 28–43.

Gordon, S.J. & Dorn, R.I. 2005. *In situ* weathering rind erosion. *Geomorphology*, **67**, 97–113.

Griffiths, R.I., Whiteley, A.S., O'donnell, A.G. & Bailey, M.J. 2000. Rapid method for coextraction of DNA and RNA from natural environments for analysis of ribosomal DNA- and rRNA-based microbial community composition. *Applied and Environmental Microbiology*, **66**, 5488–5491.

Hildebrand, A.R. 1993. The Cretaceous/Tertiary Boundary Impact (or the dinosaurs didn't have a chance). *Journal of the Royal Astronomical Society of Canada*, **87**, 77–117.

Hodgson, J.M. 1976. *Soil Survey Field Handbook*. Soil Survey Technical Monograph, **5**.

Huber, M.S & Koeberl, C. 2012. Distribution of meteoritic material in Sudbury ejecta. *Meteoritics and Planetary Science Supplement*, id.5136.

Kalm, V., Kriiska, A. & Aruväli, J. 1997. Mineralogical analysis applied in provenance studies of Estonian Neolithic pottery. *Eesti NSV Teaduste Akadeemia Toimetised, Geoloogia*, **1**, 16–34.

Kennett, J.P., Becker, L. & West, A. 2007. Triggering of the Younger Dryas Cooling by extraterrestrial impact. *American Geophysical Union, Annual Meeting*, PP41A-05.

Kennett, D.J., Kennett, J.P., *et al.* 2009. Nanodiamonds in the Younger Dryas boundary sediment. *Science*, **323**, 94.

Langworthy, K.A., Krinsley, D.H. & Dorn, R.I. 2011. Investigation of Tibetian Plateau varnish: New findings at the nanoscale using focused ion beam and transmission electron microscopy techniques. *Scanning*, **33**, 78–81.

Laustela, M., Egli, M., Frauenfelder, R., Kääb, A., Maisch, M. & Haeberli, W. 2003. Weathering rind measurements and relative age dating of rock glacier surfaces. *In*: Phillips, M., Springman, S.M. & Arenson, L.U. (eds) *Crystalline Regions of the Eastern Swiss Alps*. *Proceedings of the 8th International Conference on Permafrost*. Swets & Zeitlinger, Lisse, 55–56.

Lowe, J.J., Rasmussen, S.O., *et al.* 2008. Synchronisation of palaeoenvironmental events in the North Atlantic region during the Last Termination: a revised protocol recommended by the INTIMATE group. *Quaternary Science Reviews*, **27**, 6–17.

Mahaney, W.C. 1990. *Ice on the Equator*. Caxton, Ellison Bay, WI.

Mahaney, W.C. 2002. *Atlas of Sand Grain Surface Textures and Applications*. Oxford University Press, Oxford.

Mahaney, W.C. 2008. *Hannibal's Odyssey: Environmental Background to the Alpine Invasion of Italia*. Gorgias, Piscataway, NJ.

Mahaney, W.C & Keiser, L. 2013. Weathering rinds: unlikely host clasts for evidence of an impact-induced event. *Geomorphology*, **184**, 74–83.

Mahaney, W.C., Milner, M.W., Kalm, V., Dirszowsky, R., Hancock, R.G.V. & Beukens, R.P. 2008. Evidence for a Younger Dryas glacial advance in the Andes of northwestern Venezuela. *Geomorphology*, **96**, 199–211.

Mahaney, W.C., Kalm, V., Kapran, B. & Hewitt, K. 2009. Clast fabric and mass wasting on asteroid 25143-Itokawa: Correlation with talus and other periglacial features on Earth. *Sedimentary Geology*, **219**, 44–57.

Mahaney, W.C., Krinsley, D. & Kalm, V. 2010. Evidence for a cosmogenic origin of fired glaciofluvial beds in the northwestern Andes: Correlation with experimentally heated quartz and feldspar. *Sedimentary Geology*, **231**, 31–40.

Mahaney, W.C., Krinsley, D.H., Dohm, J.M., Kalm, V., Langworthy, K. & Ditto, J. 2011*a*. Notes on the black mat sediment, Mucuñuque Catchment, northern Mérida Andes, Venezuela. *Journal of Advanced Microscopic Research*, **6**, 1–9.

Mahaney, W.C., Krinsley, D., *et al.* 2011*b*. Fired glaciofluvial sediment in the northwestern Andes: Biotic aspects of the black mat. *Sedimentary Geology*, **237**, 73–83.

Mahaney, W.C., Krinsley, D.H., Allen, C.C.R., Langworthy, K., Ditto, J. & Milner, M.W. 2012*a*. Weathering rind: Archives of paleoenvironments on Mount Kenya, East Africa. *Journal of Geology*, **120**, 591–602.

Mahaney, W.C., Dohm, J.M., Fairen, A. & Krinsley, D.H. 2012*b*. Weathering rinds on clasts: Examples from Earth and Mars as short and long term recorders of paleoenvironment. *Journal of Planetary and Space Sciences*, **73**, 243–253.

Mahaney, W.C., Krinsley, D.H. & Allen, C.C.R. 2013*a*. Biomineralization of weathered rock rinds: Examples from the lower Afroalpine zone on Mount Kenya. *Geomicrobiology*, doi:10.1080/01490451.2012.705952.

Mahaney, W.C., Barendregt, R.W., Hamilton, T.S., Hancock, R.G.V., Tessler, D. & Costa, P.J.M. 2013*b*. Stratigraphy of the Gorges Moraine System, Mount Kenya: palaeosol and paleoclimate record. *Journal of the Geological Society, London* (in press).

Muyzer, G., De Waal, E.C. & Uitterlinden, A.G. 1993. Profiling of complex microbial populations by denaturing gradient gel electrophoresis analysis of polymerase chain reaction-amplified genes coding for 16S rRNA. *Applied and Environmental Microbiology*, **59**, 695–700.

National Soil Survey Center. 1995. *Soil Survey Laboratory Information Manual*. Soil Survey Investigations Report, **45**, Version 1.00.

Napier, W.M. 2010. Palaeolithic extinctions and the Taurid Complex. *Monthly Notices of the Royal Astronomical Society*, **405**, 1901–1906.

Navarre-Stichler, A., Steefel, C.I., Sak, P.B. & Brantley, S.L. 2011. A reactive-transport model for weathering rind formation on basalt. *Geochimica et Cosmochimica Acta*, **75**, 7644–7667.

Nicholson, D.T. 2008. Rock control on microweathering of bedrock surfaces in a periglacial environment. *Geomorphology*, **101**, 655–665.

Nicholson, D.T. 2009. Holocene microweathering rates and processes on ice-eroded bedrock, Røldal area, Hardangervidda, southern Norway. *In*: Knight, J. & Harrison, S. (eds) *Periglacial and Paraglacial Processes and Environments*. Geological Society, London, Special Publications, **320**, 29–49.

Oguchi, C.T. 2004. A porosity-related diffusion model of weathering-rind development. *Catena*, **58**, 65–75.

Oguchi, C.T. & Matsukura, Y. 2000. Effect of porosity on the increase in weathering-rind thicknesses of andesite gravel. *Developments in Geotechnical Engineering*, **84**, 305–317.

Oyama, M & Takehara, H. 1970. *Standard Soil Color Charts*. Japan Research Council for Agriculture, Forestry and Fisheries, Tokyo.

Pelt, E., Chabaux, F., Innocent, C., Navarre-Sitchler, A.K., Sak, P.B. & Brantley, S.L. 2003. Uranium–thorium chronometry of weathering rinds:

Rock alteration rate and paleo-isotopic record of weathering fluids. *Earth and Planetary Science Letters*, **276**, 98–105.

Pinter, N. & Ishman, S.E. 2008. Impacts, mega-tsunami, and other extraordinary claims. *GSA Today*, **18**, 37–38.

Quade, J., Forester, R.M., Pratt, W.L. & Carter, C. 1998. Black mats, spring-fed streams, and Late Glacial Age recharge in the southern Great Basin. *Quaternary Research*, **49**, 129–148.

Ralska-Jasiewiczowa, M., Stebich, M. & Negendank, J.F.W. 2001. Correlation and synchronization of Lateglacial continental sequences in northern central Europe based on annually laminated lacustrine sediments. *Quaternary Science Reviews*, **20**, 1233–1249.

Ricker, K.E., Chinn, T.J. & McSaveney, M.J. 1993. A late Quaternary moraine sequence dated by rock weathering rinds, Craigieburn Range, New Zealand. *Canadian Journal of Earth Sciences*, **30**, 1861–1869.

Rudnick, R.L. & Gao, S. 2005. Composition of the continental crust. *In*: Rudnick, R.L. (ed.) *The Crust: Treatise on Geochemistry*. Elsevier, Amsterdam, 1–64.

Ryerson, F.J. & Watson, E.B. 1987. Rutile saturation in magmas: Implications for Ti–Nb–Ta depletion in island-arc basalts. *Earth and Planetary Science Letters*, **86**, 225–239.

Sak, P.B., Fisher, D.M., Gardner, T.W., Murphy, K. & Brantley, S.L. 2004. Rates of weathering rind formation on Costa Rican basalt. *Geochimica et Cosmochimica Acta*, **68**, 1453–1472.

Schloss, P.D. & Handelsmann, J. 2006. Toward a consensus of bacteria in soil. *PLOS Computational Biology*, **2**, e92, doi:10.1371/journal.pcbi.0020092.

Sharp, R.P. 1969. Semiquantitative differentiation of glacial moraines near Convict Lake, Sierra Nevada, Calif. *Journal of Geology*, **77**, 68–91.

Stebbins, J.F. & Du, L.-S. 2002. Chloride ion sites in silicate and aluminosilicate glasses: A preliminary study by ^{35}Cl solid state NMR. *American Mineralogist*, **87**, 359–363.

Teller, J.T., Leverington, D.W. & Mann, J.D. 2002. Freshwater outbursts to the oceans from glacial Lake Agassiz and their role in climate change during the last deglaciation. *Quaternary Science Reviews*, **21**, 879–887.

Thorn, C.E.J.D. 1975. Influence of late-lying snow on rock-weathering rinds. *Arctic and Alpine Research*, **7**, 373–378.

Vance Haynes, C. 2008. Younger Dryas 'black mats' and the Rancholabrean termination in North America. *Proceedings of the National Academy of Sciences of the USA*, **105**, 6520–6525.

Vanderhammen, T. & Hooghiemstra, H. 1995. The El Abra Stadial, A Younger Dryas equivalent in Colombia. *Quaternary Science Reviews*, **14**, 841–851.

Vanderhammen, T. & Vangeel, B. 2008. Charcoal in soils of the Allerød–Younger Dryas transition were the result of natural fires and not necessarily the effect of an extra-terrestrial impact. *Netherlands Journal of Geosciences*, **87**, 359–361.

Vortisch, W., Mahaney, W.C. & Fecher, K. 1987. Lithology and weathering in a palaeosol sequence on Mt. Kenya, East Africa. *Geologica et Paleontologica*, **21**, 245–255.

Wittke, J.H., Weaver, J.C., *et al.* 2013. Evidence for deposition of 10 million tonnes of cosmic impact spherules across four continents 12,800 years ago. *Proceedings of the National Academy of Sciences of the USA*, http://dx.doi.org/10.1073/pnas.1301760110.

Received 4 January 2013; revised typescript accepted 25 April 2013.
Scientific editing by Quentin Crowley.

The Geological Society

serving science & profession

TAKE THAT NEXT STEP TO FAST TRACK YOUR CAREER...BECOME A **CHARTERED GEOLOGIST** OR **CHARTERED SCIENTIST**

- A peer reviewed process which requires a high standard of knowledge, competence and professionalism
- The hallmark of professional achievement, recognised in the UK and in an expanding number of countries
- Identifies you as competent and professional in your chosen speciality, and binds you to an enforced Code of Conduct
- Recognises your achievement within your industry and among your peers
- In some sectors Chartered Geologists can sign off legal papers and reports
- Chartered Geologist makes you eligible to apply for the title of European Geologist

Contact us today and request an information pack to charter your flight to success

www.geolsoc.org.uk/chartership

Fellowship Department, The Geological Society, Burlington House, Piccadilly, London W1J 0BG
Tel: 020 7434 9944 Fax: 020 7439 8975
Email: **enquiries@geolsoc.org.uk**

Background image: ©Fugro NPA, Oman